inorganics

MDPI

Article

Softening the Donor-Set: From [Cu(P^P)(N^N)][PF_6] to [Cu(P^P)(N^S)][PF_6]

Isaak Nohara, Alessandro Prescimone, Catherine E. Housecroft and Edwin C. Constable *

Department of Chemistry, University of Basel, BPR 1096, Mattenstrasse 24a, CH-4058 Basel, Switzerland; Isaak.nohara@unibas.ch (I.N.); Alessandro.prescimone@unibas.ch (A.P.); catherine.housecroft@unibas.ch (C.E.H.)

* Correspondence: edwin.constable@unibas.ch; Tel.: +41-61-207-1001

Received: 17 December 2018; Accepted: 15 January 2019; Published: 18 January 2019

Abstract: We report the synthesis and characterization of [Cu(P^P)(N^S)][PF_6] complexes with P^P = bis(2-(diphenylphosphino)phenyl) ether (POP) or 4,5-bis(diphenylphosphino)-9,9- dimethylxanthene (xantphos) and N^S = 2-(*iso*-propylthio)pyridine (*i*PrSpy) or 2-(*tert*-butylthio)pyridine (*t*BuSpy). The single crystal structures of [Cu(POP)(*i*PrSPy)][PF_6] and [Cu(POP)(*t*BuSPy)][PF_6] have been determined and confirm a distorted tetrahedral copper(I) centre and chelating P^P and N^S ligands in each complex. Variable temperature (VT) ^{1}H and ^{31}P{^{1}H} NMR spectroscopy reveals dynamic behavior with motion of the POP backbone in [Cu(POP)(*i*PrSPy)][PF_6] and [Cu(POP)(*t*BuSPy)][PF_6] frozen out at 238 K. VT NMR spectroscopic data including EXSY peaks in the ROESY spectrum of [Cu(xantphos)(*t*BuSPy)][PF_6] at 198 K reveal that two conformers exist in an approximate ratio of 5:1. Replacing bpy by the N^S ligands shifts the Cu^+/Cu^{2+} oxidation to a higher potential. The copper(I) compounds are weak emitters in the solid state with PLQY values of <2%. These values are similar to those for [Cu(POP)(bpy)][PF_6] and [Cu(xantphos)(bpy)][PF_6] in the solid state.

Keywords: Copper; coordination complex; 2-(alkylthio)pyridine; bis(phosphane); X-ray structure; dynamic behavior

1. Introduction

Around forty years ago, McMillin and co-workers reported the photoluminescence of the metal-to-ligand charge transfer (MLCT) state of copper(I) complexes containing both diimine (2,2′-bipyridine, bpy or 1,10-phenanthroline, phen) and PPh_3 or chelating bis(phosphane) ligands [1,2]. Since then, the field has extended to applications of [Cu(P^P)(N^N)]$^+$ complexes (N^N = diimine chelates and P^P = bis(phosphane) [3,4] and to the use of copper(I) complexes containing *N*-heterocyclic carbenes [5,6] as emitters in light-emitting electrochemical cells (LECs). Many [Cu(P^P)(N^N)]$^+$ compounds exhibit thermally activated delayed fluorescence (TADF), meaning that the energy gap between the singlet and triplet excited states is small enough to permit repopulation of the singlet from the triplet state under ambient conditions. This leads to indirect harvesting of triplet-state fluorescence, thereby improving LEC performance [7–12]. In [Cu(P^P)(N^N)]$^+$ cations, the lowest unoccupied molecular orbital (LUMO) is localized on the N^N ligand and the emissive properties of these compounds are typically tuned by structural and electronic manipulation of the N^N domain [3,4,13]. The highest occupied molecular orbital (HOMO) of [Cu(P^P)(N^N)]$^+$ is largely centered on copper with small contributions from phosphorus, and structural variation within the P^P domain is expected to affect steric rather than electronic properties [14], and the P–Cu–P bite angle is critical in understanding the detailed structure and properties of a [Cu(P^P)(N^N)]$^+$ complex [15]. The most commonly encountered P^P ligands are 4,5-bis(diphenylphosphino)-9, 9-dimethylxanthene (xantphos) and bis(2-(diphenylphosphino)phenyl)ether (POP) (Scheme 1), both of which are commercially available.

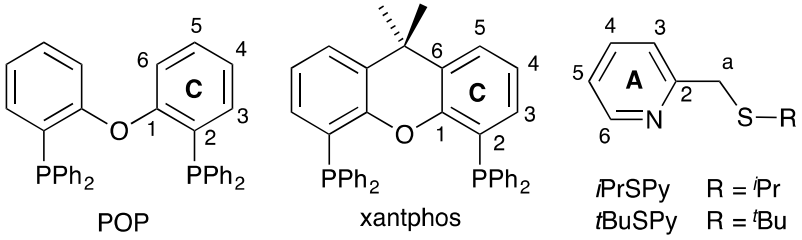

Scheme 1. Structures of POP, xantphos and the NˆS ligands with ring and atom numbering for NMR spectroscopic assignments. The phenyl rings in the PPh_2 groups of POP and xantphos are labelled D. (The ring labels are chosen to allow comparison with our previous work, for example, see References [13,14]).

Most investigations of copper(I) complexes for applications in LECs continue to focus on $[Cu(P^{\wedge}P)(N^{\wedge}N)]^+$ compounds, and we were interested to note that relatively little attention has been paid to copper(I) complexes containing PR_3 or bis(phosphane) ligands in combination with hard-soft chelating NˆS donors. A number of $[Cu(PPh_3)_2(N^{\wedge}S)]$ and related compounds, in which H(NˆS) is a thiosemicarbazone, have been described [16–20], and there are several reports of thiocyanato-bridged dicopper(I) compounds, for example $[Cu_2(PPh_3)_2(2\text{-Mepy})_2(\mu\text{-NCS})_2]$ [21], which present a distorted tetahedral CuP_2NS coordination sphere. Copper(I) complexes incorporating heterocyclic thioamide and phosphane ligands have also been described [22,23], and are shown to exhibit broad emission bands in the range λ^{em}_{max} = 490–495 nm (λ_{exc} = 270–291 nm) [21]. $[Cu_2(dppdtbpf)_2(\mu\text{-NCS})_2]$ (dppdtbpf = 1-diphenylphosphino-1′-di-*tert*-butylphosphinoferrocene) exhibits a broad emission with $\lambda^{em}_{max} \approx 500$ nm assigned to a metal-centered transition [24]. However, detailed studies of the emission behavior of $[Cu(PR_3)_2(N^{\wedge}S)]^+$ complexes are, to the best of our knowledge, absent from the literature. We were therefore motivated to investigate a series of compounds that combined simple NˆS chelates with the POP and xantphos ligands.

2. Results and Discussion

2.1. Preliminary Theoretical Investigation

Before embarking on a synthetic study, we examined the ground state electronic structure of the model $[Cu(POP)(MeSPy)]^+$ cation shown in Figure 1. After geometry optimization, DFT calculations revealed a similar partitioning of orbital character in the HOMO and LUMO, as has been shown for $[Cu(N^{\wedge}N)(P^{\wedge}P)]^+$ (see Introduction). The LUMO of $[Cu(POP)(MeSPy)]^+$ is localized on the NˆS domain and largely on the pyridine ring (Figure 1a), while the HOMO displays dominant copper character with smaller contributions from the ligands (Figure 1b). These results suggested that the LUMO energy of $[Cu(P^{\wedge}P)(N^{\wedge}S)]^+$ complexes may be modified by structural modification of the NˆS domain.

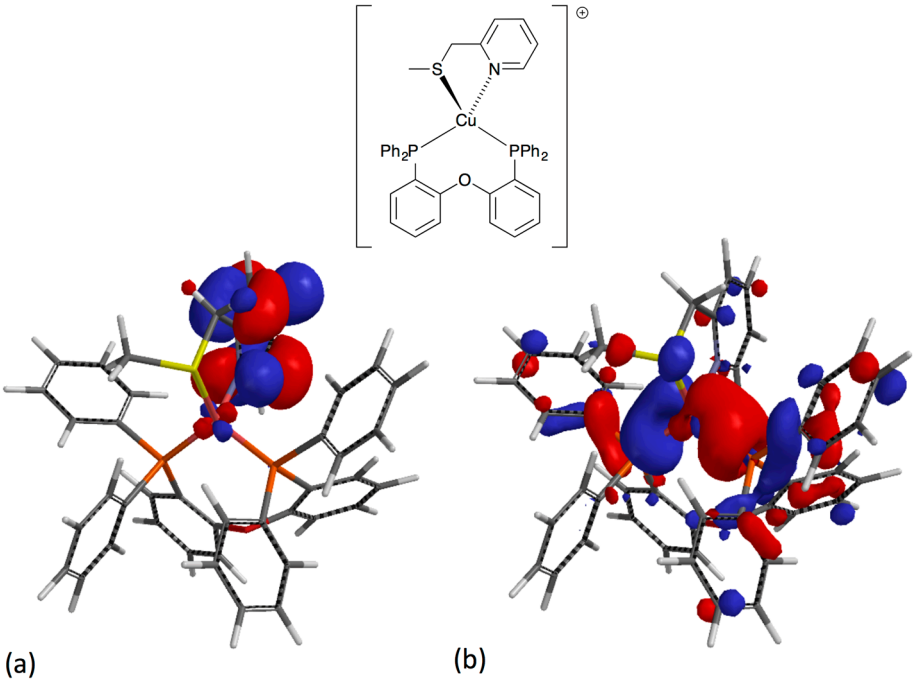

Figure 1. Characters of the (**a**) LUMO and (**b**) HOMO of the model [Cu(POP)(N^S)]$^+$ compound shown, and calculated at a DFT level (6-31G* basis set in vacuum).

2.2. Synthesis of Ligands and Copper(I) Complexes

For an initial investigation, we chose the N^S ligands *i*PrSPy and *t*BuSPy shown in Scheme 1. They were prepared by following literature procedures and the ^{1}H and ^{13}C{^{1}H} NMR spectra (Figures S1 and S2) were in agreement with those reported [25,26]. The heteroleptic [Cu(P^P)(N^S)][PF_6] complexes were obtained by addition of the N^S ligand to a CH_2Cl_2 solution containing a 1:1 mixture of [Cu(MeCN)$_4$][PF_6] and the P^P ligand. The [Cu(P^P)(N^S)][PF_6] compounds were isolated as colourless solids in 41% to 67% yield. The base peak in the positive mode electrospray mass spectrum of each compound arose from the [M–PF_6]$^+$ ion (see Materials and Methods Section).

2.3. Structural Characterizations

Colourless single crystals of [Cu(POP)(*i*PrSPy)][PF_6] and [Cu(POP)(*t*BuSPy)][PF_6] were grown by diffusion of Et_2O into acetone solutions of the complexes. Both compounds crystallize in the monoclinic $P2_1/c$ space group. Figure 2 and Figure S3 depict the cations in the two compounds. In [Cu(POP)(*i*PrSPy)][PF_6] (Figure S3), the phenyl ring with C40 was disordered and was modelled over two sites with 65% and 35% occupancies. A disorder involving the *i*PrSPy ligand was modelled over two equal-occupancy sites; the S atom was common to both ligand positions. The crystal structures confirm the κ^2*N*,*S*-binding modes of *i*PrSPy and *t*BuSPy and the distorted tetrahedral geometry of copper(I). Selected bond parameters are given in the captions to Figure 2 and Figure S3 and are unexceptional. The unit cell dimensions for the two compounds are comparable (see Materials and Methods Section) and the similarity between the ligand conformations in the [Cu(POP)(*i*PrSPy)]$^+$ and [Cu(POP)(*t*BuSPy)]$^+$ cations is seen in Figure 3. Each cation is chiral and both enantiomers are present in the unit cell. No intracation π-stacking of aromatic rings is observed in either [Cu(POP)(*i*PrSPy)]$^+$ or [Cu(POP)(*t*BuSPy)]$^+$. This contrasts with the numerous examples of structurally characterized salts of [Cu(POP)(N^N)]$^+$ and [Cu(xantphos)(N^N)]$^+$ complexes that exhibit intracation π-stacking [27]. It is noteworthy that the PM3 optimized geometry of the model [Cu(POP)(MeSPy)]$^+$ cation, shown in Figure 1, also exhibited no π-stacked pairs of aromatic rings.

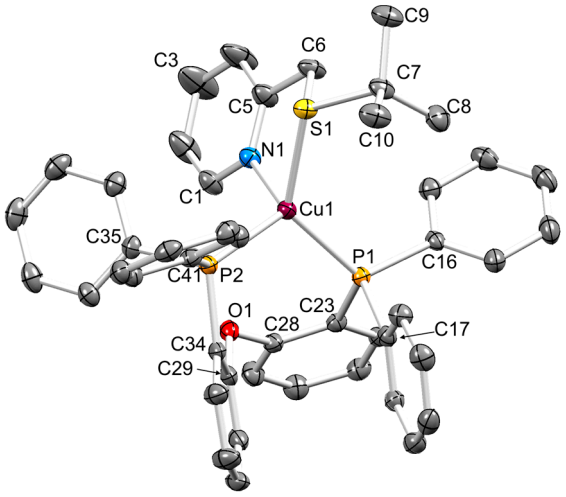

Figure 2. ORTEP-style diagram of the structure of the [Cu(POP)(*t*BuSPy)]$^+$ cation in [Cu(POP)(*t*BuSPy)][PF_6]. Ellipsoids plotted at 40% probability level and H atoms omitted for clarity. Selected bond parameters: Cu1–S1 = 2.3332(7), Cu1–N1 = 2.099(2), Cu1–P1 = 2.2584(7), Cu1–P2 = 2.2817(8), C6–S1 = 1.823(3), C7–S1 = 1.856(3), C28–O1 = 1.400(3), C29–O1 = 1.395(3) Å; S1–Cu1–N1 = 83.17(7), S1–Cu1–P1 = 126.12(3), N1–Cu1–P1 = 107.37(7), S1–Cu1–P2 = 113.79(3), N1–Cu1–P2 = 111.10(7), P1–Cu1–P2 = 110.81(3), C7–S1–C6 = 102.93(14), C7–S1–Cu1 = 121.62(10), C6–S1–Cu1 = 95.28(10), and C28–O1–C29 = 115.1(2)°.

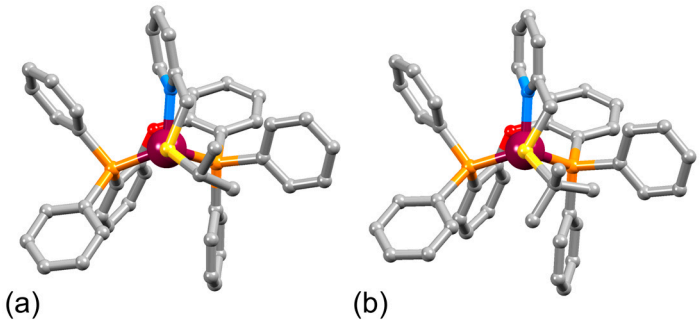

Figure 3. Comparison of the structures of the (**a**) [Cu(POP)(*i*PrSPy)]$^+$ and (**b**) [Cu(POP)(*t*BuSPy)]$^+$ cations, each viewed along the S–Cu bond.

2.4. NMR Spectroscopic Characterization and Solution Dynamics

The solution NMR spectra of the compounds were recorded in acetone-d_6. The complexes are kinetically stable in this solvent with respect to ligand redistribution, at least for the period of data collection. Atom labelling for the NMR assignments is given in Schemes 1 and 2. The solution $^{31}P\{^1H\}$ NMR spectrum of each [Cu(P^P)(N^S)][PF_6] compound at 298 K (Figure S4) showed a broadened singlet arising from POP or xantphos (δ −12.6 ppm for each POP-containing compound, and δ −13.1 and −14.4 ppm for [Cu(xantphos)(*i*PrSPy)][PF_6] and [Cu(xantphos)(*t*BuSPy)][PF_6], respectively) in addition to a septet from the [PF_6]$^-$ ion. At 298 K, the solution ^1H NMR spectra (Figures S5–S8) contained sharp signals for the N^S ligands, with broadened signals from POP or xantphos being indicative of dynamic behavior. In addition, the coordinated sulfur atom (which is a stereogenic center) can undergo inversion. As in the crystallographically determined structure of the cations shown in Figure 3, the two P atoms in these [Cu(P^P)(N^S)]$^+$ complexes would be inequivalent if inversion at sulfur were frozen out. Since this was never observed in the low temperature $^{31}P\{^1H\}$ NMR spectra (see below), we conclude that inversion at the coordinated-S atom is a low energy process in all four complexes.

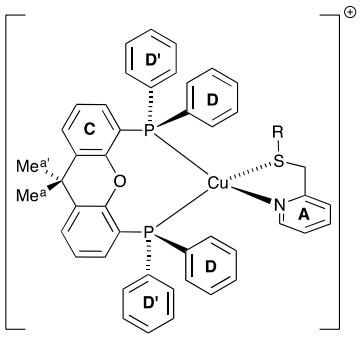

Scheme 2. Inequivalence of the phenyl rings in each PPh_2 group and of the xantphos methyl groups in $[Cu(RSPy)(xantphos)]^+$. A similar inequivalence occurs in $[Cu(RSPy)(POP)]^+$.

Over the temperature range 298–238 K, the ^1H NMR spectra of $[Cu(POP)(i\text{PrSPy})][PF_6]$ and $[Cu(POP)(t\text{BuSPy})][PF_6]$ remain essentially unchanged in the alkyl region as shown for $[Cu(POP)(t\text{BuSPy})][PF_6]$ in Figure S9. Figure 4 and Figure S10 show the aromatic regions of the variable temperature spectra of $[Cu(POP)(i\text{PrSPy})][PF_6]$ and $[Cu(POP)(t\text{BuSPy})][PF_6]$, respectively, and reveal that signals assigned to the protons of the phenyl rings, which are broad at 298 K, are partly resolved into two sets (labelled D and D′) at 238 K. Exchange (EXSY) cross-peaks are observed in the ROESY spectrum at 238 K between signals for the pairs of protons $H^{D2}/H^{D'2}$ and $H^{D3}/H^{D'3}$, as shown for $[Cu(POP)(t\text{BuSPy})][PF_6]$ in Figure 5. A low intensity NOESY cross-peak is observed in the ROESY spectrum between protons H^{D2} and H^{A6}, and this is displayed for $[Cu(POP)(t\text{BuSPy})][PF_6]$ in Figure S11. There is no corresponding NOESY correlation between H^{A6} and $H^{D'2}$, indicating that the D rings point up towards to N^S ligand while the D′ rings are directed away (see Figure 3 and Scheme 2). For a molecular weight of around 700, NOESY peaks in a ROESY spectrum are expected to have a close to zero intensity [28]. In summary, dynamic processes in $[Cu(POP)(i\text{PrSPy})][PF_6]$ and $[Cu(POP)(t\text{BuSPy})][PF_6]$ involve motion of the POP backbone that is frozen out at 238 K, while inversion at the coordinated sulfur atom is still rapid on the NMR timescale at 238 K.

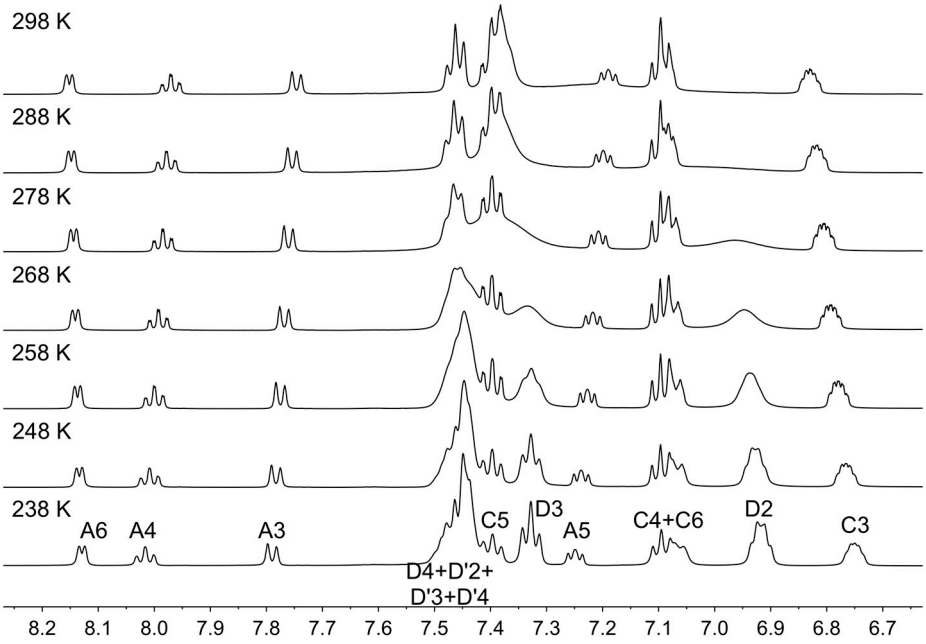

Figure 4. Aromatic region in the variable temperature ^1H NMR spectra of $[Cu(POP)(i\text{PrSPy})][PF_6]$ (500 MHz, acetone-d_6).

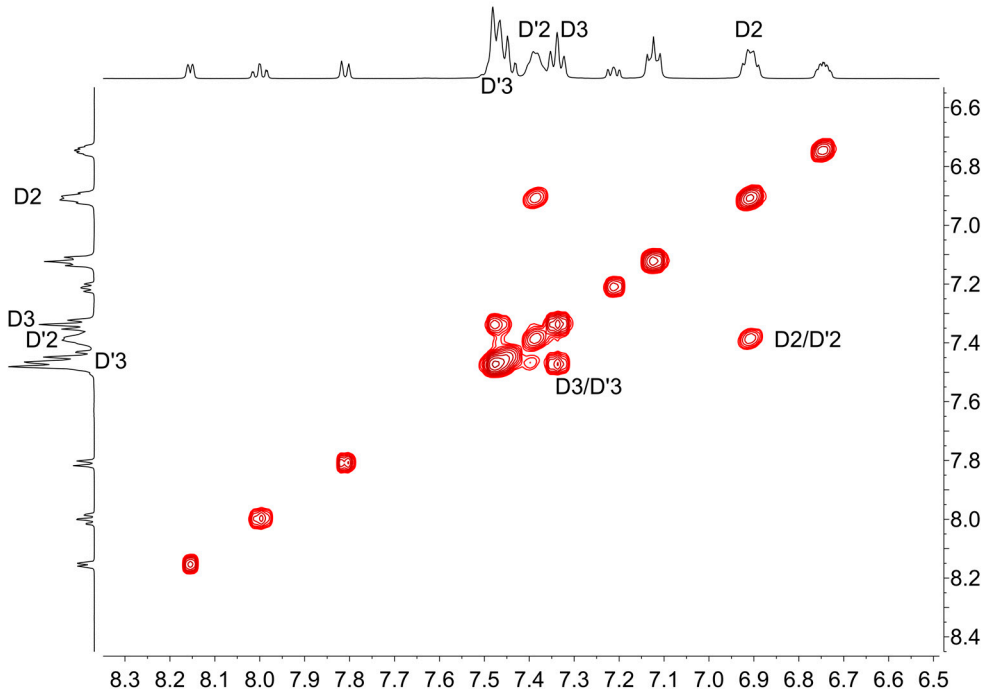

Figure 5. EXSY peaks in the ROESY spectrum of [Cu(POP)(*t*BuSPy)][PF_6] (500 MHz, acetone-d_6, 238 K).

The xantphos ligand has less flexibility than POP, because of the insertion of the CMe_2 bridge across the back of the ligand (Scheme 1). However, we have previously detailed dynamic processes involving the inversion of the xanthene unit in coordinated xantphos, which leads to the interconversion of, for example, conformers of [Cu(xantphos)(Phbpy)]$^+$ [29] and of [Cu(xantphos)(1-Pyrbpy)]$^+$ [30], (Phbpy = 6-phenyl-2,2′-bipyridine, 1-Pyrbpy = 6-(1-pyrenyl)-2,2′-bipyridine). For [Cu(xantphos)(*t*BuSPy)][PF_6], the broad $^{31}P\{^1H\}$ NMR signal at 298 K from the xantphos ligand (δ −14.4 ppm) is replaced at 198 K by two signals at δ −16.8 and −10.4 ppm with relative integrals of 5:1 (Figure S12). This integral ratio is the same as that observed for signals arising from two species present in the ^1H NMR spectrum of [Cu(xantphos)(*t*BuSPy)][PF_6] at 198 K (Figure 6 for the aromatic region and Figure S13 for the alkyl region). COSY, ROESY, HMQC, and HMBC spectra recorded at 198 K were used to assign the major peaks in the spectrum, and EXSY peaks in the ROESY spectrum at 198 K were used to correlate the major and minor species. The EXSY peaks for [Cu(xantphos)(*t*BuSPy)][PF_6] are instructive. Figure 7 shows the aromatic region and reveals the very different environments of proton H^{A6} of the pyridine ring (Scheme 2) in the two species. The EXSY peaks shown in Figure 8 verify the exchange between the *tert*-butyl groups of the two species, as well as the exchange between the inner and outer pointing methyl groups of the xantphos CMe_2 units in the two species. This can only occur if the xanthene unit undergoes the inversion, as shown in Scheme 3, for one pair of possible conformers. In summary for [Cu(xantphos)(*t*BuSPy)][PF_6], two species are present in solution at 198 K, assigned to conformers which interconvert at higher temperatures through inversion of the xanthene "bowl"; fast inversion at the coordinated sulfur atom occurs on the NMR timescale at 198 K.

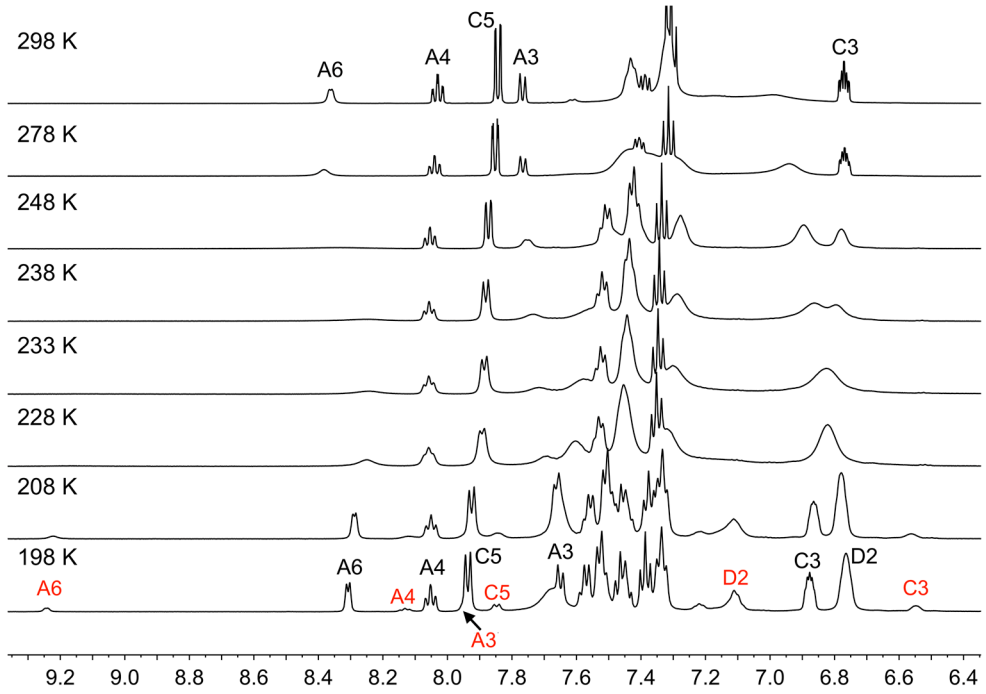

Figure 6. Aromatic region in the variable temperature ^{1}H NMR spectra of [Cu(xantphos)(*t*BuSPy)][PF_6] (500 MHz, acetone-d_6). At 198 K, the major species is represented by black labels, and minor species by red labels. See Materials and Methods Section for full assignment of major species.

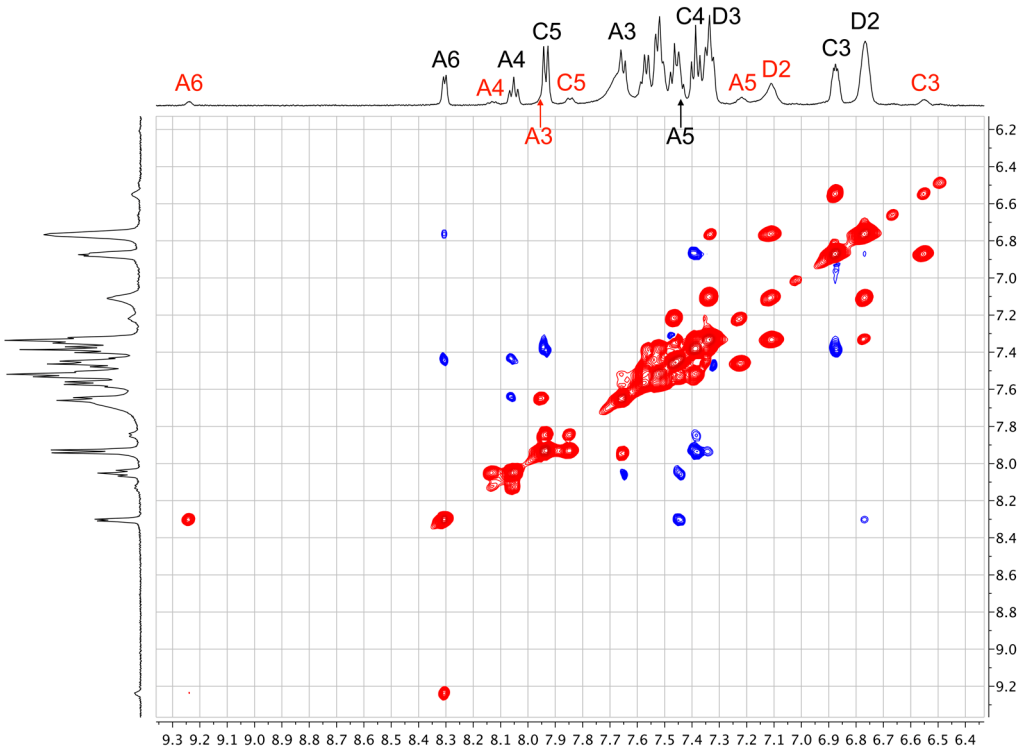

Figure 7. EXSY (red) and NOESY (blue) cross-peaks in the aromatic region of the ROESY spectrum of [Cu(xantphos)(*t*BuSPy)][PF_6] (500 MHz, acetone-d_6, 198 K). Major species represented by black labels, minor by red labels. See Materials and Methods Section for full assignment of major species.

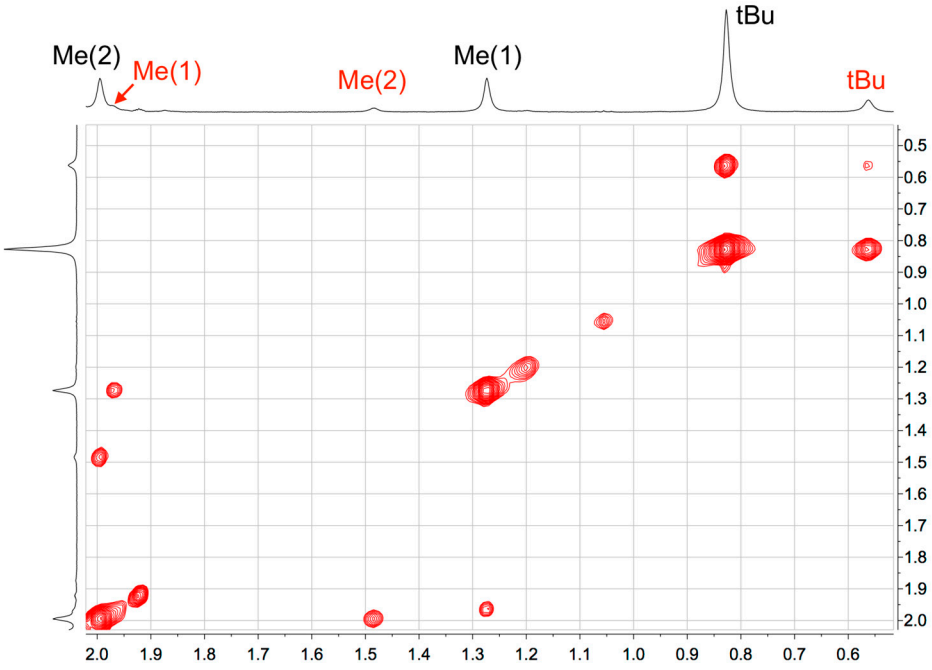

Figure 8. EXSY cross-peaks in the alkyl region of the ROESY spectrum of [Cu(xantphos)(*t*BuSPy)][PF_6] (500 MHz, acetone-d_6, 198 K). Major species represented by black labels, minor by red labels.

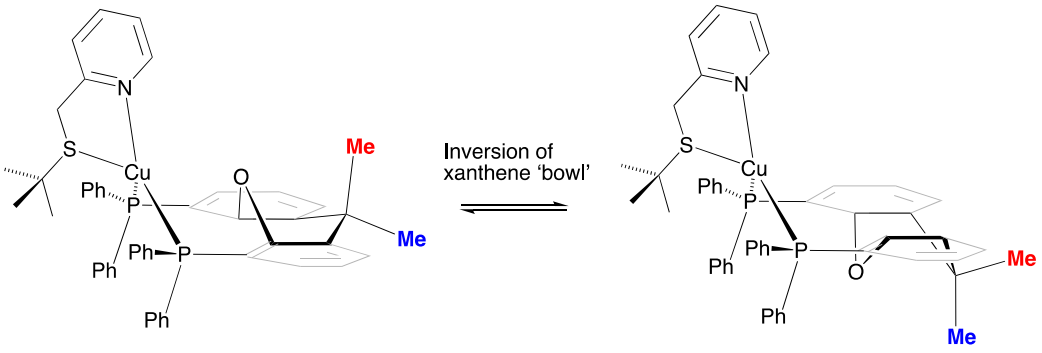

Scheme 3. Possible conformers of [Cu(xantphos)(*t*BuSPy)]$^+$ and interconversion through inversion of the xanthene unit.

2.5. Electrochemistry

Cyclic voltammetry was used to investigate the electrochemistry of the copper(I) complexes. Each undergoes a quasi-reversible or irreversible oxidation, which is assigned to a Cu^+/Cu^{2+} process (Table 1 and Figures S14 and S15). For the benchmark-compounds [Cu(POP)(bpy)][PF_6] and [Cu(xantphos)(bpy)][PF_6], the Cu^+/Cu^{2+} process occurs at +0.72 and +0.76 V, respectively [13]. Thus, replacing bpy by the N^S ligands shifts the oxidation to a higher potential. This observation results from an interplay of two opposing effects. A change from bpy to the less π-accepting N^S ligands should make Cu^+ easier to oxidize, whereas the soft *S*-donor favours the copper(I) oxidation state. If the forward CV scan is taken past about +1.1 V, a second (irreversible) oxidation process, assigned to phosphane oxidation, is observed. No reduction processes were observed in the cyclic voltammograms within the solvent accessible window.

Table 1. Cyclic voltammetry data for [Cu(P^P)(N^S)][PF_6] complexes in CH_2Cl_2 (1–5 × 10^{-3} M, vs. Fc^+/Fc, [$^nBu_4N$][PF_6] as supporting electrolyte, scan rate = 0.1 V s^{-1}).

Compound	$E_{1/2}^{ox}$/V	(E_{pc}–E_{pa}/mV)
[Cu(POP)(*i*PrSPy)][PF_6]	+0.86	220
[Cu(POP)(*t*BuSPy)][PF_6]	+0.96	irreversible
[Cu(xantphos)(*i*PrSPy)][PF_6]	+1.02	220
[Cu(xantphos)(*t*BuSPy)][PF_6]	+0.92	240

2.6. Photophysical Properties

Figure 9 displays the solution absorption spectra of the [Cu(P^P)(N^S)][PF_6] complexes. For comparison, the absorption spectra of the N^S ligands are shown in Figure S16; the absorption spectra of POP and xantphos have previously been reported [31]. The compounds are colourless, and the intense high-energy absorption bands (Table 2) are assigned to ligand-based, spin-allowed π*←π and π*←*n* transitions. The compounds are non-emissive in solution, and solid samples excited at 280 nm gave emission maxima between 470 and 490 nm (Table 2 and Figure S17), blue-shifted with respect to the reference compounds [Cu(POP)(bpy)][PF_6] and [Cu(xantphos)(bpy)][PF_6] (λ_{em}^{max} = 581 and 587 nm with $\lambda_{excitation}$ = 365 nm [13]). The solid-state photoluminescence quantum yields (PLQY) are <2% (Table 2), which is significantly lower than for many [Cu(P^P)(N^N)][PF_6] compounds, for example [13,27,29,30]. However, it is important to note that PLQY values for [Cu(POP)(bpy)][PF_6] and [Cu(xantphos)(bpy)][PF_6] are also low in the solid state (3.0% and 1.7%, respectively [13]), and that enhancement of PLQY is only achieved by tuning the substitution pattern of the bpy ligand [13,27,29].

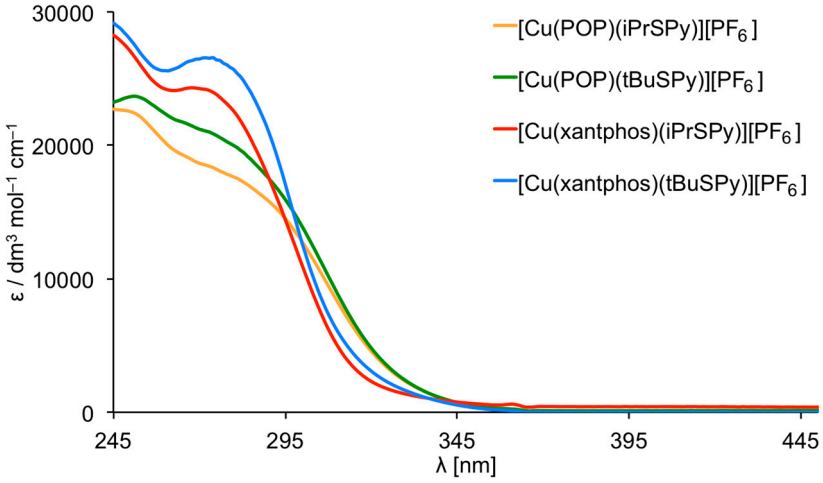

Figure 9. Absorption spectra of CH_2Cl_2 solutions of [Cu(P^P)(N^S)][PF_6] complexes (concentration = 2.5 × 10^{-5} mol dm^{-3}).

Table 2. Solution (CH_2Cl_2, 2.5 × 10^{-5} mol dm^{-3}) absorption maxima and solid-state emission data for [Cu(P^P)(N^S)][PF_6].

Complex Cation	Solution Absorption	Solid-State Emission	
	λ_{abs}^{max}/nm (ε/L mol^{-1} cm^{-1})	λ_{em}^{max}/nm ($\lambda_{excitation}$/nm)	PLQY/% ($\lambda_{excitation}$)
[Cu(*i*PrSPy)(POP)]$^+$	248 (22,600), 280 (17,600)	470 (280)	<1% (280)
[Cu(*t*BuSPy)(POP)]$^+$	250 (23,600), 275 (20,700)	490 (280)	<1% (280)
[Cu(*i*PrSPy)(xantphos)]$^+$	269 (24,300)	475 (280)	<2% (280)
[Cu(*t*BuSPy)(xantphos)]$^+$	272 (26,600)	490 (280)	<1% (280)

3. Materials and Methods

3.1. General

^{1}H, ^{13}C{^{1}H} and ^{31}P{^{1}H} NMR spectra were recorded on a Bruker Avance 500 spectrometer (Bruker BioSpin AG, Fällanden, Switzerland); spectra for the ligands were recorded at 295 K, spectra for the complexes were recorded at 238 K unless otherwise stated. ^{1}H and ^{13}C NMR chemical shifts were referenced to the residual solvent peaks with respect to δ(TMS) = 0 ppm and ^{31}P NMR chemical shifts and with respect to δ(85% aqueous H_3PO_4) = 0 ppm.

Solution absorption and emission spectra were measured using an Agilent 8453 spectrophotometer (Agilent Technologies Inc., Santa Clara, CA, USA) and a Shimadzu RF-5301PC spectrofluorometer (Shimadzu Schweiz GmbH, Roemerstr., Switzerland), respectively. A Shimadzu LCMS-2020 instrument or a Bruker esquire 3000plus instrument was used to record electrospray ionization (ESI) mass spectra. Quantum yields (CH_2Cl_2 solution and powder) were measured using a Hamamatsu absolute photoluminescence (PL) quantum yield spectrometer C11347 Quantaurus-QY. Powder emission spectra were measured with a Hamamatsu Compact Fluorescence lifetime Spectrometer C11367 Quantaurus-Tau, using an LED light source with λ_{exc} = 280. Electrochemical measurements were carried out using a CH Instruments 900B potentiostat with [^{n}Bu$_4$N][PF_6] (0.1 M) as the supporting electrolyte and at a scan rate of 0.1 V s^{-1}. The working electrode was glassy carbon, the reference electrode was a leakless Ag^+/AgCl (eDAQ ET069-1) and the counter-electrode platinum wire. Final potentials were internally referenced with respect to the Fc/Fc^+ couple ($E_{1/2}$ = 1.126 V with respect to Ag/AgCl at 298.15 K [32]).

POP and xantphos were purchased from Acros (Chemie Brunschwig AG, Basel, Switzerland) and Fluorochem (Hadfield, UK), respectively. [Cu(MeCN)$_4$][PF_6] was prepared by the published method [33]. The N^S ligands were prepared according to the literature and the NMR spectroscopic data matched with those reported [25,26].

3.2. [Cu(POP)(iPrSPy)][PF_6]

[Cu(MeCN)$_4$][PF_6] (0.23 g, 0.62 mmol) and POP (0.33 g, 0.62 mmol) were dissolved in CH_2Cl_2 (40 mL). The reaction mixture was stirred at room temperature for 2 h, then 2-((*iso*-propylthio)methyl)pyridine (0.10 g, 0.62 mmol) was added by syringe. Then the reaction mixture was stirred for 1 h and subsequently the solvent was removed under reduced pressure. The crude product was washed with Et_2O and crystallized by vapour diffusion of Et_2O into a CH_2Cl_2 solution of the compound. [Cu(POP)(*i*PrSPy)][PF_6] was obtained as colourless crystals (0.38 g, 0.41 mmol, 67%). ^{1}H NMR (500 MHz, acetone-d_6, 248 K) δ/ppm 8.13 (d, J = 5.1 Hz, 1H, H^{A6}), 8.01 (td, J = 7.7, 1.7 Hz, 1H, H^{A4}), 7.78 (d, J = 7.8 Hz, 1H, H^{A3}), 7.52–7.42 (m, 12, $H^{D4+D'2+D'3+D'4}$), 7.40 (m, 2H, H^{C5}), 7.33 (m, 4H, H^{D3}), 7.24 (m, 1H, H^{A5}), 7.14–7.00 (m, 4H, H^{C4+C6}), 6.98–6.84 (m, 4H, H^{D2}), 6.77 (m, 2H, H^{C3}), 4.13 (s, 2H, H^{a}), 2.57 (septet, J = 6.6 Hz, 1H, $H^{Pr\text{-}CH}$), 0.97 (d, J = 6.6 Hz, 5H, $H^{Pr\text{-}Me}$). ^{13}C{^{1}H} NMR (126 MHz, acetone-d_6, 248 K) δ/ppm 158.3 (C^{C1}), 156.3 (C^{A2}), 149.8 (C^{A6}), 139.5 (C^{A4}), 134.7 (C^{C3}), 134.5/132.9/129.3 ($C^{D'2,3,4}$), 132.9 (C^{C5}), 132.7 (C^{D2}), 131.2 ($C^{D'1}$), 130.7 (C^{D4}), 130.0/125.7 (C^{C6+C4}), 129.5 (C^{D3}), 125.5 (C^{D1}), 125.1 (C^{A3}), 124.6 (C^{A5}), 120.8 (C^{C2}), 38.6 ($C^{a+Pr\text{-}CH}$), 21.9 ($C^{Pr\text{-}Me}$). ^{31}P{^{1}H} NMR (202 MHz, acetone-d_6, 298 K) δ/ppm −12.6 (broad, FWHM = 170 Hz), −144.3 (septet, J_{PF} = 710 Hz). ESI-MS: m/z 768.2 $[M - PF_6]^+$ (base peak, calc. 768.2). Found: C 58.97, H 4.73, N 1.61; and $C_{45}H_{41}CuF_6NOP_3S$ requires C 59.11, H 4.52, N 1.53.

3.3. [Cu(xantphos)(iPrSPy)][PF_6]

[Cu(MeCN)$_4$][PF_6] (0.23 g, 0.62 mmol) and xantphos (0.36 g, 0.62 mmol) were dissolved in CH_2Cl_2 (40 mL). The reaction mixture was stirred at room temperature for 2 h, then 2-((*iso*-propylthio)methyl)pyridine (0.10 mg, 0.62 mmol) was added by syringe. Then, the reaction mixture was stirred for 1 h and then the solvent was removed under reduced pressure. The crude product was washed with Et_2O to yield [Cu(xantphos)(*i*PrSPy)][PF_6] as a colourless solid (0.32 g,

0.35 mmol, 57%). ^{1}H NMR (500 MHz, acetone-d_6, 238 K) Major species (see text): δ/ppm 8.11–7.98 (m, 2H, H^{A6+A4}), 7.88 (d, J = 7.7 Hz, 2H, H^{C5}), 7.73 (d, J = 7.8 Hz, 1H, H^{A3}), 7.53–7.39 (m, 12H, $H^{D4+D'2+D'3+D'4}$), 7.38–7.27 (m, 7H, $H^{A5+C4+D3}$), 6.84 (m, 4H, H^{D2}), 6.74 (m, 2H, H^{C3}), 3.74 (s, 2H, H^{a}), 2.60 (m, 1H, H^{iPr-H}), 1.95 (s, 3H $H^{xantphos-Me}$), 1.40 (s, 3H $H^{xantphos-Me}$), 0.89–0.86 (m, 6H, H^{Pr-Me}). ^{13}C{^{1}H} NMR (126 MHz, acetone-d_6, 238 K) δ/ppm 156.8 (C^{A2}), 155.1 (C^{C1}), 149.8 (C^{A6}), 140.1 (C^{A4}), 134.4 (C^{C6}), 134.3/130.9/129.9 ($C^{D4+D'2+D'3+D'4}$), 132.9 (C^{D2}), 132.8 (C^{D1}), 132.0 (C^{C3}), 131.4 ($C^{D'1}$), 129.8 (C^{D3}), 129.0 (C^{C5}), 125.8 (C^{A3+C4}), 125.7 (C^{A5}), 120.1 (C^{C2}), 39.0 (C^{a}), 38.5 (C^{Pr-CH}), 36.4 ($C^{xantphos\ bridge}$), 32.0/24.9 ($C^{xantphos-Me}$), and 21.8 (C^{Pr-Me}). ^{31}P{^{1}H} NMR (202 MHz, acetone-d_6, 298 K) δ/ppm −13.1 (broad, FWHM = 200 Hz), −144.3 (septet, J_{PF} = 710 Hz). ESI-MS: m/z 808.2 $[M - PF_6]^+$ (base peak, calc. 808.2). Found: C 61.06, H 4.89, N 1.48; $C_{48}H_{45}CuF_6NOP_3S$ requires C 60.41, H 4.75, N 1.47.

3.4. [Cu(POP)(tBuSPy)][PF$_6$]

$[Cu(MeCN)_4][PF_6]$ (0.20 g, 0.62 mmol) and POP (0.30 g, 0.62 mmol) were dissolved in CH_2Cl_2 (40 mL). The reaction mixture was stirred at room temperature for 2 h, then 2-((*tert*-butylthio)methyl)pyridine (0.10 g, 0.55 mmol) was added by syringe. Then the reaction mixture was stirred for 1h and subsequently the solvent was removed under reduced pressure. The crude product was washed with Et_2O and crystallized by vapour diffusion of Et_2O into a CH_2Cl_2 solution of the product. [Cu(POP)(*t*BuSPy)][PF_6] was obtained as colourless crystals (0.21 g, 0.23 mmol, 41%). ^{1}H NMR (500 MHz, acetone-d_6, 238 K) δ/ppm 8.15 (d, J = 5.0 Hz, 1H, H^{A6}), 8.00 (td, J = 7.7, 1.5 Hz, 1H, H^{A4}), 7.81 (d, J = 8.0 Hz, 1H, H^{A3}), 7.52–7.42 (m, 10H, $H^{C5+D4+D'3+D'4}$), 7.42–7.37 (m, 4H, $H^{D'2}$), 7.34 (m, 4H, H^{D3}), 7.24–7.17 (m, 1H, H^{A5}), 7.16–7.06 (m, 4H, H^{C4+C6}), 6.97–6.86 (m, 4H, H^{D2}), 6.79–6.70 (m, 2H, H^{C3}), 4.25 (s, 2H, H^{a}), 1.01 (s, 9H, H^{t-Bu}). ^{13}C{^{1}H} NMR (126 MHz, acetone-d_6, 238 K) δ/ppm 158.8 (C^{C1}), 157.4 (C^{A2}), 149.9 (C^{A6}), 139.6 (C^{A4}), 135.0 (C^{C3}), 134.7 ($C^{D'1}$), 134.5 ($C^{D'2}$), 133.2 (C^{C5+D1}), 133.1 ($C^{D'3+D'4}$), 132.9 (C^{D2}), 129.9 (C^{D4}), 129.6 (C^{D3}), 125.8 ($C^{C6/C4}$), 121.0 ($C^{C6/C4}$), 125.1 (C^{A3}), 124.5 (C^{A5}), 124.1 (C^{C2}), 47.8 (C^{Bu-Cq}), 37.7 (C^{a}), 29.5 (C^{t-Bu}) ^{31}P{^{1}H} NMR (202 MHz, acetone-d_6, 298 K) δ/ppm −12.6 (broad, FWHM = 170 Hz), −144.3 (septet, J_{PF} = 710 Hz). ESI-MS: m/z 782.2 $[M - PF_6]^+$ (base peak, calc. 782.2). Found: C 59.43, H 4.76, N 1.70; $C_{46}H_{43}CuF_6NOP_3S$ requires C 59.51, H 4.67, N 1.53.

3.5. [Cu(xantphos)(tBuSPy)][PF$_6$]

$[Cu(MeCN)_4][PF_6]$ (0.23 g, 0.62 mmol) and xantphos (0.32 g, 0.62 mmol) were dissolved in CH_2Cl_2 (40 mL). The reaction mixture was stirred at room temperature for 2 h, then 2-((*tert*-butylthio)methyl)pyridine (0.10 g, 0.55 mmol) was added by syringe. Then the reaction mixture was stirred for 1 h and subsequently the solvent was removed under reduced pressure. The crude product was washed with Et_2O to give [Cu(xantphos)(*t*BuSPy)][PF_6] as a colourless solid (0.28 g, 0.28 mmol, 51%). ^{1}H NMR (500 MHz, acetone-d_6, 198 K) major species (see text, integrals of some signals are affected by minor species and are not stated): δ/ppm 8.31 (d, J = 5.1 Hz, 1H, H^{A6}), 8.05 (t, J = 7.3 Hz, 1H, H^{A4}), 7.94 (d, J = 7.6 Hz, 2H, H^{C5}), 7.74–7.62 (m, $H^{A3+D'4}$), 7.60–7.49 (m, $H^{D'2+D'3}$), 7.49–7.42 (m, H^{A5+D4}), 7.39 (m, 2H, H^{C4}), 7.34 (m, 4H, H^{D3}), 6.88 (m, 2H, H^{C3}), 6.80–6.73 (m, 4H, H^{D2}), 3.40 (s, 2H, H^{a}), 2.00 (s, 3H, $H^{xantphos-Me}$), 1.27 (s, 3H, $H^{xantphos-Me}$), 0.83 (s, 9H, H^{t-Bu}). ^{13}C{^{1}H} NMR (126 MHz, acetone-d_6, 198 K) δ/ppm 157.7 (C^{A2}), 154.7 (C^{C1}), 149.5 (C^{A6}), 139.7 (C^{A4}), 134.5 ($C^{D'4}$), 133.9 (C^{C6}), 132.3 (C^{C3}), 132.1 (C^{D2}), 131.4 ($C^{D'2/D'3}$), 130.5 (C^{D4}) 130.4 (C^{D1}), 129.6 ($C^{D'2/D'3}$), 129.4 (C^{D3}), 129.0 (C^{C5}), 125.4 (C^{C4}), 124.9 ($C^{D'1}$), 124.8 (C^{A5}), 124.5 (C^{A3}), 119.6 (C^{C2}), 47.9 (C^{Bu-Cq}), 36.9 (C^{a}), 35.9 ($C^{xantphos-bridge}$), 33.0 ($H^{xantphos-Me}$), 23.8 ($H^{xantphos-Me}$), 28.7 (C^{t-Bu}). ^{31}P{^{1}H} NMR (202 MHz, acetone-d_6, 298 K) δ/ppm −14.4 (broad, FWHM = 175 Hz), −144.3 (septet, J_{PF} = 710 Hz). ESI-MS: m/z 822.2 $[M - PF_6]^+$ (base peak, calc. 822.2). Found: C 60.82, H 4.95, N 1.55; $C_{49}H_{47}CuF_6NOP_3S$ requires C 60.77, H 4.89, N 1.45.

3.6. Crystallography

Data were collected on a Bruker Kappa Apex2 diffractometer (Bruker Biospin AG, Fällanden, Switzerland) with data reduction, solution and refinement using the programs APEX [34]

and CRYSTALS [35]. Structural analysis was carried out using Mercury v. 3.5.1 [36,37]. In [Cu(POP)(*i*PrSPy)][PF_6], the disordered rings were refined as rigid bodies, and the disordered pyridine ring had to be refined isotropically.

[Cu(POP)(*i*PrSPy)][PF_6]: $C_{45}H_{41}CuF_6NOP_3S$, M = 914.35, colourless block, monoclinic, space group $P2_1/c$, a = 14.0474(11), b = 17.4236(14), c = 18.3028(13) Å, β = 109.786(2)°, U = 4215.2(6) Å^3, Z = 4, D_c = 1.441 Mg m^{-3}, μ(Cu-Kα) = 2.810 mm^{-1}, T = 123 K. Total 33404 reflections, 7650 unique, R_{int} = 0.028. Refinement of 7275 reflections (541 parameters) with $I > 2\sigma(I)$ converged at final R_1 = 0.0743 (R_1 all data = 0.0762), wR_2 = 0.1724 (wR_2 all data = 0.1728), gof = 0.9944. CCDC 1871032.

[Cu(POP)(*t*BuSPy)][PF_6]: $C_{46}H_{40}CuF_6NOP_3S$, M = 928.37, colourless block, monoclinic, space group $P2_1/c$, a = 13.8102(4), b = 18.4985(6), c = 18.0974(6) Å, β = 107.7455(16)°, U = 4403.3(2) Å^3, Z = 4, D_c = 1.400 Mg m^{-3}, μ(Cu-Kα) = 2.699 mm^{-1}, T = 123 K. Total 25698 reflections, 7939 unique, R_{int} = 0.030. Refinement of 6739 reflections (532 parameters) with $I > 2\sigma(I)$ converged at final R_1 = 0.0530 (R_1 all data = 0.0617), wR_2 = 0.1350 (wR_2 all data = 0.1388), gof = 0.9911. CCDC 1871033.

3.7. Density Functional Theory (DFT) Calculations

Ground state DFT calculations were carried out using Spartan 16 (v. 2.0.10) [38] at the B3LYP level with a 6-31G* basis set in vacuum. Although the choice of atomic orbital basis set (6-311++G** basis set on all atoms, 6-311++G** on Cu and 6-31G* basis set on C, H and N, or 6-31G* basis set on all atoms) greatly influences the calculated absorption spectra of related copper(I) dyes, the MO characteristics are little affected [39], and therefore a 6-31G* basis set on all atoms was selected to optimize computer time. Initial geometry energy optimization was carried out at a semi-empirical (PM3) level.

4. Conclusions

We have prepared and characterized [Cu(POP)(*i*PrSPy)][PF_6], [Cu(POP)(*t*BuSPy)][PF_6], [Cu(xantphos)(*i*PrSPy)][PF_6] and [Cu(xantphos)(*t*BuSPy)][PF_6] with the aim of comparing their structures and spectroscopic properties with those of the benchmark compounds [Cu(POP)(bpy)][PF_6] and [Cu(xantphos)(bpy)][PF_6]. The single crystal structures of [Cu(POP)(*i*PrSPy)][PF_6] and [Cu(POP)(*t*BuSPy)][PF_6] confirm a distorted tetrahedral environment for copper(I) and the presence of PˆP and NˆS chelating ligands. Variable temperature ^{1}H and ^{31}P{^{1}H} NMR spectroscopic investigations demonstrate that dynamic processes in [Cu(POP)(*i*PrSPy)][PF_6] and [Cu(POP)(*t*BuSPy)][PF_6] involve motion of the POP backbone which is frozen out at 238 K. For [Cu(xantphos)(*t*BuSPy)][PF_6], two conformers are present in acetone solution and at 198 K, signal integrals in both the ^{31}P{^{1}H} and ^{1}H NMR spectra show that the ratio of these species is ~5:1. Exchange between the species has been confirmed through the observation of EXSY peaks in the ROESY spectrum. In all four compounds, inversion at the coordinated stereogenic sulfur atom is rapid on the NMR timescale over the temperature ranges studied. Replacing bpy by the NˆS ligands shifts the Cu^+/Cu^{2+} oxidation to higher potential. All the copper compounds are weak emitters in the solid state, but PLQY values of <2% are of the same order of magnitude as for [Cu(POP)(bpy)][PF_6] and [Cu(xantphos)(bpy)][PF_6]. Since enhancement of emission behaviour in [Cu(POP)(NˆN)][PF_6] and [Cu(xantphos)(NˆN)][PF_6] where NˆN is a derivative of bpy is critically dependent upon ligand functionalization [13,27,29] we are motivated to further investigate [Cu(PˆP)(NˆS)][PF_6] complexes which show noteworthy kinetic stability with respect to ligand redistribution in acetone solutions.

Supplementary Materials: The following are available online at http://www.mdpi.com/2304-6740/7/1/11/s1, Figures S1 and S2: ^{1}H NMR spectra of *i*PrSPy and *t*BuSPy. Figure S3: ORTEP-style plot of the [Cu(POP)(*i*PrSPy)]$^+$ cation. Figure S4: ^{31}P{^{1}H} NMR spectra of the complexes at 298 K. Figures S5–S13: Additional ^{1}H, ^{31}P{^{1}H} NMR and ROESY spectra. CCDC numbers are for the structures of [Cu(POP)(^{i}PrSPy)][PF_6] and [Cu(POP)(^{t}BuSPy)][PF_6]. Figures S14 and S15: Cyclic voltammograms of the complexes. Figure S16: Solution absorption spectra of *i*PrSPy and *t*BuSPy. Figure S17: Solid-state emission spectra. The CIF and checkCIF files of [Cu(POP)(*i*PrSPy)][PF_6] and [Cu(POP)(*t*BuSPy)][PF_6].

Author Contributions: I.N.: Synthesis and compound characterization, data management; A.P.: crystallography; C.E.H.: manuscript writing, project concepts, data interpretation; E.C.C.: project concepts, data interpretation, contributions to manuscript.

Funding: This research was funded by The Swiss National Science Foundation (grant numbers 200020_162631 and 200020_182000) and the University of Basel.

Acknowledgments: Daniel Häussinger (University of Basel) is thanked for assistance with low temperature NMR spectroscopy.

Conflicts of Interest: The authors declare no conflict of interest.

References

1. Buckner, M.T.; McMillin, D.R. Photoluminescence from copper(I) complexes with low-lying metal-to-ligand charge transfer excited states. *J. Chem. Soc. Chem. Commun.* **1978**, 759–760. [CrossRef]
2. Rader, R.A.; McMillin, D.R.; Buckner, M.T.; Matthews, T.G.; Casadonte, D.J.; Lengel, R.K.; Whittaker, S.B.; Darmon, L.M.; Lytle, F.E. Photostudies of 2,2′-bipyridine bis(triphenylphosphine)copper(1+), 1,10-phenanthroline bis(triphenylphosphine)copper(1+), and 2,9-dimethyl-1,10-phenanthroline bis(triphenylphosphine)copper(1+) in solution and in rigid, low-temperature glasses. Simultaneous multiple emissions from intraligand and charge-transfer states. *J. Am. Chem. Soc.* **1981**, *103*, 5906–5912. [CrossRef]
3. Costa, R.D.; Ortí, E.; Bolink, H.J.; Monti, F.; Accorsi, G.; Armaroli, N. Luminescent ionic transition metal complexes for light-emitting electrochemical cells. *Angew. Chem. Int. Ed.* **2012**, *51*, 8178–8211. [CrossRef] [PubMed]
4. Elie, M.; Gaillard, S.; Renaud, J.-L. *Light-Emitting Electrochemical Cells: Concepts, Advances and Challenges*; Costa, R.D., Ed.; Springer: Cham, Switzerland, 2017; Chapter 11; p. 287.
5. Elie, M.; Sguerra, F.; Di Meo, F.; Weber, M.D.; Marion, R.; Grimault, A.; Lohier, J.-F.; Stallivieri, A.; Brosseau, A.; Pansu, R.B.; et al. Designing NHC–copper(I) dipyridylamine complexes for blue light-emitting electrochemical cells. *ACS Appl. Mater. Interfaces* **2016**, *8*, 14678–14691. [CrossRef] [PubMed]
6. Weber, M.D.; Fresta, E.; Elie, M.; Miehlich, M.E.; Renaud, J.-L.; Meyer, K.; Gaillard, S.; Costa, R.D. Rationalizing fabrication and design toward highly efficient and stable blue light-emitting electrochemical cells based on NHC copper(I) complexes. *Adv. Funct. Mater.* **2018**, *28*, 1707423. [CrossRef]
7. Liu, J.; Oliva, J.; Tong, K.; Zhao, F.; Chen, D.; Pei, Q. Multi-colored light-emitting electrochemical cells based on thermal activated delayed fluorescense host. *Sci. Rep.* **2017**, *7*, 1524. [CrossRef]
8. Leitl, M.J.; Krylova, V.A.; Djurovich, P.I.; Thompson, M.E.; Yersin, H. Phosphorescence versus thermally activated delayed fluorescence. Controlling singlet–triplet splitting in brightly emitting and sublimable Cu(I) compounds. *J. Am. Chem. Soc.* **2014**, *136*, 16032–16038. [CrossRef]
9. Czerwieniec, R.; Yersin, H. Diversity of copper(I) complexes showing thermally activated delayed fluorescence: Basic photophysical analysis. *Inorg. Chem.* **2015**, *54*, 4322–4327. [CrossRef]
10. Hofbeck, T.; Monkowius, U.; Yersin, H. Highly efficient luminescence of Cu(I) compounds: Thermally activated delayed fluorescence combined with short-lived phosphorescence. *J. Am. Chem. Soc.* **2015**, *137*, 399–404. [CrossRef]
11. Czerwieniec, R.; Leitl, M.J.; Homeier, H.H.H.; Yersin, H. Cu(I) complexes—Thermally activated delayed fluorescence. Photophysical approach and material design. *Coord. Chem. Rev.* **2016**, *325*, 2–28. [CrossRef]
12. Yersin, H.; Czerwieniec, R.; Shafikov, M.Z.; Suleymanova, A.F. TADF material design: Photophysical background and case studies focusing on Cu^I and Ag^I complexes. *ChemPhysChem* **2017**, *18*, 3508–3535. [CrossRef]
13. Keller, S.; Brunner, F.; Junquera-Hernández, J.M.; Pertegás, A.; La-Placa, M.-G.; Prescimone, A.; Constable, E.C.; Bolink, H.J.; Ortí, E.; Housecroft, C.E. CF_3 Substitution of [Cu(P^P)(bpy)][PF_6] complexes: Effects on photophysical properties and light-emitting electrochemical cell performance. *ChemPlusChem* **2018**, *83*, 217–229. [CrossRef]
14. Brunner, F.; Babaei, A.; Pertegás, A.; Junquera-Hernández, J.M.; Prescimone, A.; Constable, E.C.; Bolink, H.J.; Sessolo, M.; Ortí, E.; Housecroft, C.E. Phosphane tuning in heteroleptic [Cu(N^N)(P^P)]$^+$ complexes for light-emitting electrochemical cells. *Dalton Trans.* **2019**, *48*, 446–460. [CrossRef] [PubMed]
15. Leoni, E.; Mohanraj, J.; Holler, M.; Mohankumar, M.; Nierengarten, I.; Monti, F.; Sournia-Saquet, A.; Delavaux-Nicot, B.; Nierengarten, J.-F.; Armaroli, N. Heteroleptic copper(I) complexes prepared from

phenanthroline and bis-phosphine ligands: Rationalization of the photophysical and electrochemical properties. *Inorg. Chem.* **2018**, *57*, 15537–15549. [CrossRef] [PubMed]
16. Belicchi-Ferrari, M.; Bisceglie, F.; Buluggiu, E.; Pelosi, G.; Tarasconi, P. Investigations into bis(triphenylphosphine)copper(I) complexes with cyclic derivatives of methylpyruvate thiosemicarbazones. *Polyhedron* **2010**, *29*, 2134–2141. [CrossRef]
17. Lobana, T.S.; Indoria, S.; Sharma, M.; Nandi, J.; Jassal, A.K.; Hundal, M.S.; Castineiras, A. Synthesis, structure and spectroscopy of mono- and di-nuclear copper(I) complexes incorporating anionic thiophene based thiosemicarbazones-first examples. *Polyhedron* **2014**, *80*, 34–40. [CrossRef]
18. Hakimi, M.; Moeini, K.; Mardani, Z.; Takjoo, R. Synthesis and Spectral Study of a Copper(I) Complex, [Cu(L)(PPh3)2], with NS-Donor Ligand. *Phosphorus Sulfur Silicon* **2014**, *189*, 596–605. [CrossRef]
19. Ramachandran, R.; Prakash, G.; Vijayan, P.; Viswanathamurthi, P.; Malecki, J.G. Synthesis of heteroleptic copper(I) complexes with phosphine-functionalized thiosemicarbazones: An efficient catalyst for regioselective N-alkylation reactions. *Inorg. Chim. Acta* **2017**, *464*, 88–93. [CrossRef]
20. Lobana, T.S.; Kaushal, M.; Virk, R.K.; Garcia-Santos, I.; Jasinski, J.P. Thiosemicarbazonates of copper: Crystal structures of [(furan-2-acetaldehyde-*N*-phenyl-thiosemicarbazonato)][bis(triphenylphosphine)] copper(I) and [bis(furan-2-formaldehyde-*N*-phenyl-thiosemicarbazonato)]copper(II). *Polyhedron* **2018**, *152*, 49–54. [CrossRef]
21. Pettinari, C.; di Nicola, C.; Marchetti, F.; Pettinari, R.; Skelton, B.W.; Somers, N.; White, A.H.; Robinson, W.T.; Chierotti, M.R.; Gobetto, R.; et al. Synthesis, characterization, spectroscopic and photophysical properties of new [Cu(NCS){(L-*N*)$_2$ or (L′-*NN*)}(PPh$_3$)] complexes (L-*N*, L′-*NN* = aromatic nitrogen base). *Eur. J. Inorg. Chem.* **2008**, *2008*, 1974–1984. [CrossRef]
22. Batsala, G.K.; Dokorou, V.; Kourkoumelis, N.; Manos, M.J.; Tasiopoulos, A.J.; Mavromoustakos, T.; Simčič, M.; Golič-Grdadiłnik, S.; Hadjikakou, S.K. Copper(I)/(II) or silver(I) ions towards 2-mercaptopyrimidine: An exploration of a chemical variability with possible biological implication. *Inorg. Chim. Acta* **2012**, *382*, 146–157. [CrossRef]
23. Lobana, T.S.; Sandhu, A.K.; Sultana, R.; Castineiras, A.; Butcher, R.J.; Jasinski, J.P. Coordination variability of Cu^{I} in multidonor heterocyclic thioamides: Synthesis, crystal structures, luminescent properties and ESI-mass studies of complexes. *RSC Adv.* **2014**, *4*, 30511–30522. [CrossRef]
24. Trivedi, M.; Ujjain, S.K.; Singh, G.; Kumar, A.; Dubey, S.K.; Rath, N.P. Syntheses, characterization, and electrochemistry of compounds containing 1-diphenylphosphino-1′-(di-tert-butylphosphino) ferrocene (dppdtbpf). *J. Organomet. Chem.* **2014**, *772–773*, 202–209. [CrossRef]
25. Canovese, L.; Visentin, F.; Uguagliati, P.; Chessa, G.; Pesce, A. Palladium(II) allyl complexes with nitrogen–sulfur bidentate ligands. Substituent effects in the mechanism of allyl amination. *J. Organomet. Chem.* **1998**, *566*, 61–71. [CrossRef]
26. Garg, K.; Paris, S.I.M.; Rack, J.J. A Flexible Chelate Leads to Phototriggered Isomerization in an Osmium Sulfoxide Complex. *Eur. J. Inorg. Chem.* **2013**, *2013*, 1142–1148. [CrossRef]
27. Alkan-Zambada, M.; Keller, S.; Martínez-Sarti, L.; Prescimone, A.; Junquera-Hernández, J.M.; Constable, E.C.; Bolink, H.J.; Sessolo, M.; Ortí, E.; Housecroft, C.E. [Cu(P^P)(N^N)][PF$_6$] compounds with bis(phosphane) and 6-alkoxy, 6-alkylthio, 6-phenyloxy and 6-phenylthio-substituted 2,2′-bipyridine ligands for light-emitting electrochemical cells. *J. Mater. Chem. C* **2018**, *6*, 8460–8471. [CrossRef]
28. Neuhaus, D.; Williamson, M.P. *The Nuclear Overhauser Effect in Structural and Conformational Analysis*, 2nd ed.; Wiley-VCH: New York, NY, USA, 2000.
29. Keller, S.; Pertegás, A.; Longo, G.; Martinez, L.; Cerdá, J.; Junquera-Hernández, J.M.; Prescimone, A.; Constable, E.C.; Housecroft, C.E.; Ortí, E.; et al. Shine bright or live long: Substituent effects in [Cu(N^N)(P^P)]$^+$-based light-emitting electrochemical cells where N^N is a 6-substituted 2,2′-bipyridine. *J. Mater. Chem. C* **2016**, *4*, 3857–3871. [CrossRef]
30. Brunner, F.; Graber, S.; Baumgartner, Y.; Häussinger, D.; Prescimone, A.; Constable, E.C.; Housecroft, C.E. The effects of introducing sterically demanding aryl substituents in [Cu(N^N)(P^P)]$^+$ complexes. *Dalton Trans.* **2017**, *46*, 6379–6391. [CrossRef] [PubMed]
31. Pintado-Alba, A.; de la Riva, H.; Nieuwhuyzen, M.; Bautista, D.; Raithby, P.R.; Sparkes, H.A.; Teat, S.J.; López-de-Luzuriagae, J.M.; Lagunas, M.C. Effects of diphosphine structure on aurophilicity and luminescence in Au(I) complexes. *Dalton Trans.* **2004**, 3459–3467. [CrossRef]

32. Tsierkezos, N.G. Cyclic voltammetric studies of ferrocene in nonaqueous solvents in the temperaure range from 248.15 to 298.15 K. *J. Solut. Chem.* **2007**, *36*, 289–302. [CrossRef]
33. Kubas, G.J. Tetrakis(acetonitrile)copper(I) hexafluorophosphate. *Inorg. Synth.* **1979**, *19*, 90–92. [CrossRef]
34. *APEX2, Version 2 User Manual, M86-E01078*; Bruker Analytical X-ray Systems, Inc.: Madison, WI, USA, 2006.
35. Betteridge, P.W.; Carruthers, J.R.; Cooper, R.I.; Prout, K.; Watkin, D.J. CRYSTALS version 12: Software for guided crystal structure analysis. *J. Appl. Cryst.* **2003**, *36*, 1487. [CrossRef]
36. Bruno, I.J.; Cole, J.C.; Edgington, P.R.; Kessler, M.K.; Macrae, C.F.; McCabe, P.; Pearson, J.; Taylor, R. New software for searching the Cambridge Structural Database and visualizing crystal structures. *Acta Cryst. B* **2002**, *58*, 389–397. [CrossRef]
37. Macrae, C.F.; Bruno, I.J.; Chisholm, J.A.; Edgington, P.R.; McCabe, P.; Pidcock, E.; Rodriguez-Monge, L.; Taylor, R.; van de Streek, J.; Wood, P.A. Mercury CSD 2.0—New features for the visualization and investigation of crystal structures. *J. Appl. Cryst.* **2008**, *41*, 466–470. [CrossRef]
38. *Spartan 16 Version 2.0.10*; Wavefunction, Inc.: Irvine, CA, USA, 2017.
39. Bozic-Weber, B.; Chaurin, V.; Constable, E.C.; Housecroft, C.E.; Meuwly, M.; Neuburger, M.; Rudd, J.A.; Schönhofer, E.; Siegfried, L. Exploring copper(I)-based dye-sensitized solar cells: A complementary experimental and TD-DFT investigation. *Dalton Trans.* **2012**, *41*, 14157–14169. [CrossRef] [PubMed]